Electronic structure of $La_{2/3}Sr_{1/3}MnO_3$: Interplay of oxygen octahedra rotations and epitaxial strain

Martin Zahradník,[1,2,*] Thomas Maroutian,[2] Martin Zelený,[1,3] Lukáš Horák,[1] Georg Kurij,[2] Tomáš Maleček,[1] Lukáš Beran,[1] Štefan Višňovský,[1] Guillaume Agnus,[2] Philippe Lecoeur,[2] and Martin Veis[1,†]

[1]*Charles University, Faculty of Mathematics and Physics, Ke Karlovu 3, 12116 Prague 2, Czech Republic*

[2]*Centre for Nanoscience and Nanotechnology (C2N), CNRS UMR 9001, Univ Paris-Sud, Université Paris-Saclay, 91120 Palaiseau, France*

[3]*Institute of Materials Science and Engineering, NETME Centre, Faculty of Mechanical Engineering, Brno University of Technology, Technická 2896/2, 616 69 Brno, Czech Republic*

(Received 6 December 2018; revised manuscript received 21 February 2019; published 22 May 2019)

Influence of epitaxial strain and oxygen octahedra rotations on electronic structure of $La_{2/3}Sr_{1/3}MnO_3$ ultrathin films was systematically studied. The investigated films were grown by pulsed laser deposition on four different substrates: cubic (001)-oriented $LaAlO_3$, (001) $(LaAlO_3)_{1/3}(Sr_2AlTaO_6)_{2/3}$, (001) $SrTiO_3$, and orthorhombic (110) $DyScO_3$, providing a broad range of induced epitaxial strains. Magnetic properties were found to deteriorate with increasing value of the epitaxial strain, as expected due to unit cell distortion increasingly deviating from the bulk and effect of the magnetically inert layer. A combination of spectroscopic ellipsometry and magneto-optical Kerr effect spectroscopy was used to determine spectra of the diagonal and off-diagonal elements of permittivity tensor. The off-diagonal elements at room temperature confirmed the presence of two previously reported electronic transitions in the spectra of all films. Moreover they revealed another electronic transition around 4.3 eV only in the spectra of films grown under compressive strain. We proposed classification of this transition as a crystal field paramagnetic Mn $t_{2g} \rightarrow e_g$ transition. *Ab initio* calculations were employed to distinguish between the potential influence of oxygen octahedra rotations and distortions. The *ab initio* calculations indicated a negligible influence of oxygen octahedra rotations on magneto-optical properties of $La_{2/3}Sr_{1/3}MnO_3$. They further supported the proposed classification of the additional electronic transition, showing a key role of strain in controlling the electronic structure of ultrathin perovskite films.

DOI: 10.1103/PhysRevB.99.195138

I. INTRODUCTION

Hole-doped manganites $La_{1-x}M_xMnO_3$ (M = Ca, Sr, Ba) with perovskite-type structure possess unique physical properties. The colossal magnetoresistance [1] combined with a high degree of spin polarization is common for the whole family of hole-doped manganites. High scientific interest is focused on a particular case of $La_{2/3}Sr_{1/3}MnO_3$ (LSMO), which possesses the highest Curie temperature ($T_C \sim 370$ K) [2] and almost 100% spin polarization [3]. The presence of mixed valence manganese ions Mn^{3+} and Mn^{4+} leads to metallic conductivity and ferromagnetic ordering. Such a combination of physical properties makes LSMO an interesting candidate to study physical phenomena with important spintronics applications.

The ferromagnetism of LSMO is mainly driven by double-exchange (DE) interaction [4]. It originates from e_g electron transfer between Mn^{3+} and Mn^{4+} ions via O^{2-} $2p$ state. The DE electron-transfer probability strongly depends on Mn-O-Mn geometry, i.e., on Mn-O bond length and Mn-O-Mn bond angle. Therefore, the main factors influencing the magnetic properties are rotations and distortions of MnO_6 octahedra, which are induced in the LSMO films either by an epitaxial strain coming from lattice mismatched substrates or by coupling of octahedral rotations at the LSMO/substrate interface [5]. The distortions are characterized by changes of Mn-O bond lengths, while the rotations imply a tilt of the whole MnO_6 octahedron around the central manganese atom, keeping all Mn-O bond lengths constant.

The rotations of MnO_6 octahedra, or, generally, in magnetic oxides so-called oxygen octahedra rotations (OOR), have been revealed to have significant impact on resulting physical properties of these materials. There have been numerous studies trying to understand the physical mechanisms related to OOR. The fundamental research investigates origin and possible control of the OOR and its relation to epitaxial strain and crystallographic structure of the substrates [6–8]. More complex studies are trying to explain the exact impact of OOR on resulting magnetic and transport properties and to suggest possibilities of direct tuning of the physical properties by OOR engineering [9–14].

Despite all the research which points out the importance of OOR on resulting physical properties, the role of MnO_6 distortions should not be forgotten, as shown, for example, by Souza-Neto *et al.* [15,16] who presented x-ray absorption spectroscopy studies of LSMO films on $SrTiO_3$ (STO) and $LaAlO_3$ (LAO) substrates, in which they emphasized the importance of MnO_6 octahedra distortions on resulting transport and magnetic properties of the LSMO films. Therefore, we can see that although the impact of OOR and oxygen

*Corresponding author: zahradnik@karlov.mff.cuni.cz
†Corresponding author: veis@karlov.mff.cuni.cz

octahedra distortions is unequivocal, the exact nature of these phenomena and their relation to the expitaxial strain and substrate symmetry still remain unclear.

In this paper, we try to elucidate the impact of epitaxial strain on electronic structure of LSMO by means of spectroscopic ellipsometry and magneto-optical spectroscopy, which allows us to calculate spectra of both the diagonal and off-diagonal permittivity tensor elements. We investigate four ultrathin LSMO films grown on four different substrates. They induce a variety of strains in the LSMO films, ranging from large compressive strain on LAO, through small compressive strain on $(LaAlO_3)_{1/3}(Sr_2AlTaO_6)_{2/3}$ (LSAT) and small tensile strain on STO, up to large tensile strain on $DyScO_3$ (DSO). With the help of *ab initio* calculations, we were able to describe changes in electronic structure of LSMO. These changes are likely to originate from the combination of epitaxial strain and OOR.

II. EXPERIMENTAL DETAILS

Investigated LSMO films were prepared by pulsed laser deposition and their proper crystallinity and surface morphology was verified by x-ray diffraction (XRD) and atomic force microscopy (AFM), respectively. The XRD measurements were carried out using a PANanalytical X'Pert PRO diffractometer in parallel beam configuration. The AFM images were taken by a Bruker Innova AFM microscope. A set of four LSMO samples was prepared on four different substrates: LAO, LSAT, STO, and DSO. The deposition was carried out under oxygen pressure of 120 mTorr. We used a KrF laser at a wavelength of 248 nm, with typical growth rate of 15 pulses per monolayer and 2 Hz pulse-repetition rate. The substrate was kept at 900 K during the deposition process. Such parameters lead to single-crystalline growth of LSMO with low surface roughness. Thicknesses of the films were determined by XRD using the (002) Bragg reflection of LSMO fitted by classical interference formula, and these results were further verified by spectroscopic ellipsometry. Both methods confirmed that films on all four substrates are of similar thicknesses of approximately 20 nm. The presence of crystallographic twins in LAO substrate leads to lower quality of the LSMO film, resulting in the largest surface roughness of 1.4 nm. The other three samples exhibit surface roughness lower than 0.5 nm.

All investigated LSMO samples were found to be ferromagnetic at room temperature. Films grown on diamagnetic substrates of LAO, LSAT, and STO were characterized by means of SQUID magnetometry. The last substrate of DSO exhibits paramagnetism with strong magnetic anisotropy [17]. This makes characterization of magnetic properties of films grown upon its surface by purely magnetic methods nearly impossible. However magneto-optical Kerr effect (MOKE) measurements on this sample provided a clear magneto-optical signal at room temperature, unambiguously demonstrating its room temperature ferromagnetism. Lower magnitude of the MOKE in comparison to other films indicated that T_C of LSMO/DSO is close to room temperature. T_C of the other three films were determined by SQUID magnetometry as 308 K (LSMO/LAO), 361 K (LSMO/LSAT), and 340 K (LSMO/STO). See Supplemental Material [18] for the SQUID results.

Optical properties of the samples were characterized by spectroscopic ellipsometry. The measurements were carried out on a high-precision Woollam VASE ellipsometer at three angles of incidence (60°, 65°, and 70°). Both the bare substrates and the samples with deposited LSMO layers were characterized in a spectral range from 0.7 to 6.4 eV. The data were analyzed assuming a model structure of a homogeneous single LSMO layer on the corresponding substrate. The spectra of diagonal elements of permittivity tensor of the LSMO layers and their thicknesses were adjusted using the least-squares method.

Off-diagonal elements of permittivity tensor were determined by means of MOKE spectroscopy and theoretical calculations based on transfer matrix formalism [28] with use of the ellipsometric data. Room-temperature MOKE measurements were carried out using generalized magneto-optical ellipsometry with rotating analyzer in spectral range from 1.5 to 5.0 eV. All the data were recorded in polar configuration at 1 T of applied magnetic field. Such field was verified to be sufficient for complete saturation of the films. The MOKE and diagonal permittivity tensor element spectra served via transfer matrix formalism for calculations of spectra of off-diagonal permittivity tensor elements. We assumed a model of a single layer on semi-infinite substrate, which in our case is a reasonable approximation due to the unpolished back side of the substrate, having negligible contribution to optical reflection at the substrate/sample holder interface. The off-diagonal elements were then determined in spectral range between 1.5 and 5.0 eV.

Presented *ab initio* calculations were performed using the VIENNA AB INITIO SIMULATION PACKAGE (VASP) [29,30], in which the electron-ion interaction was described by projector augmented-wave potentials [31,32]. The electronic orbitals were expanded in terms of plane waves with maximum kinetic energy of 520 eV. We used the gradient-corrected exchange-correlation functional proposed by Perdew *et al.* [33,34]. We have tested that the proper account of correlation effects on Mn sites, e.g., the DFT+U method [35], does not change the main conclusions of the present paper. The Brillouin zone (BZ) was sampled using a $10 \times 10 \times 3$ Γ-point-centered mesh and integration over the BZ used the Gaussian smearing method with 0.05 eV smearing width for relaxations, while the density of states (DOS) was calculated using the tetrahedron method with Blöchl corrections [36]. The total energy was calculated with high precision by convergence to 10^{-7} eV per computational cell. The frequency-dependent complex dielectric function was calculated with the help of a methodology described in Ref. [37]. The LSMO unit cell used in *ab initio* calculations is described in the Supplemental Material [18] to avoid confusion with description of real LSMO unit cell, which follows in the next section.

III. RESULTS AND DISCUSSION

A. Structural characterization

Bulk LSMO possesses a rhombohedral unit cell with lattice parameters $a_r = 5.471$ Å and $\alpha_r = 60.43°$, but it is often described as pseudocubic with lattice parameter $a_{pc} =$

TABLE I. Lattice parameters of $La_{2/3}Sr_{1/3}MnO_3$ films grown on four different substrate materials. Calculated from reciprocal space maps measured by x-ray diffraction.

Substrate	a_m [Å]	b_m [Å]	c_m [Å]	ab [Å]	γ_m [deg]
LAO	5.510	5.512	7.582	7.581	86.92
LSAT	5.475	5.481	7.743	7.743	89.94
STO	5.474	5.475	7.807	7.808	90.97
DSO	5.474	5.475	7.891	7.890	92.24

3.876 Å [38]. The substrates we used are either (001)-oriented cubic (LAO, LSAT, and STO) with lattice parameters $a_{LAO} = 3.790$ Å, $a_{LSAT} = 3.868$ Å, and $a_{STO} = 3.905$ Å, or (110)-oriented orthorhombic (DSO) with pseudocubic lattice parameter $a_{DSO} = 3.942$ Å. Due to the lattice mismatch, the substrates impose epitaxial strain on the deposited LSMO layers. The compressive or tensile strain leads to distortion of the LSMO unit cell and can be quantified by the lattice mismatch as $(a_{layer} - a_{substr})/a_{substr}$. The LSMO unit cell under strain can be described as (110)-oriented monoclinic [39] with lattice parameters a_m, b_m, c_m, α_m, β_m, and γ_m, where $\alpha_m = \beta_m = 90°$.

Lattice parameters of the samples were determined by XRD. Reciprocal space maps (RSM) were measured around the (260), (444), (620), and (44-4) Bragg reflections for each sample. The RSM for all samples are shown in Supplemental Figs. S1– S4; they revealed fully strained LSMO films on all four substrates and allowed us to completely describe the unit cell of the LSMO films. The extracted lattice parameters are summarized in Table I and plotted in Fig. 1 as a function of the in-plane strain along $[1\text{-}10]_m$ direction.

General behavior of the lattice parameters with strain corresponds to previously published structural investigations of LSMO [6]. Distance $(ab) = \sqrt{a_m^2 + b_m^2 - 2a_m b_m \cos\gamma_m}$ represents the lateral periodicity in the $[1\text{-}10]_m$ monoclinic direction. From Table I, it can be seen that the values of the ab distance and c_m lattice parameter are almost identical for all samples, confirming that the LSMO is coherently strained in both monoclinic in-plane directions $[1\text{-}10]_m$ and $[001]_m$. Figure 1 shows the lattice parameters a_m and b_m together with the so-called orthorhombicity factor defined as b_m/a_m. In agreement with Vailionis *et al.* [6], we observe that films under compressive strain exhibit a unit cell with $a_m < b_m$ and $\gamma_m < 90°$, while for films under tensile strain $a_m \doteq b_m$ and $\gamma_m > 90°$. In the $[001]_m$ direction, both the compressive and tensile strain are accommodated by change of the c_m lattice parameter, which is strained accordingly to the respective substrate. In the $[1\text{-}10]_m$ direction, the orthorhombicity value, which is very close to unity for samples grown on STO and DSO, shows that accommodation of the tensile strain is reached only by increment of the γ_m angle. On the other hand, the compressive strain accommodates by decrease of the γ_m angle and also by relative change of the a_m and b_m lattice parameters, which can be seen as an increment of the orthorhombicity. However, the orthorhombicity does not change proportionally to the strain, in contrast to the γ_m angle and unit cell volume, which both increase almost linearly from the largest compressive to the largest tensile strain.

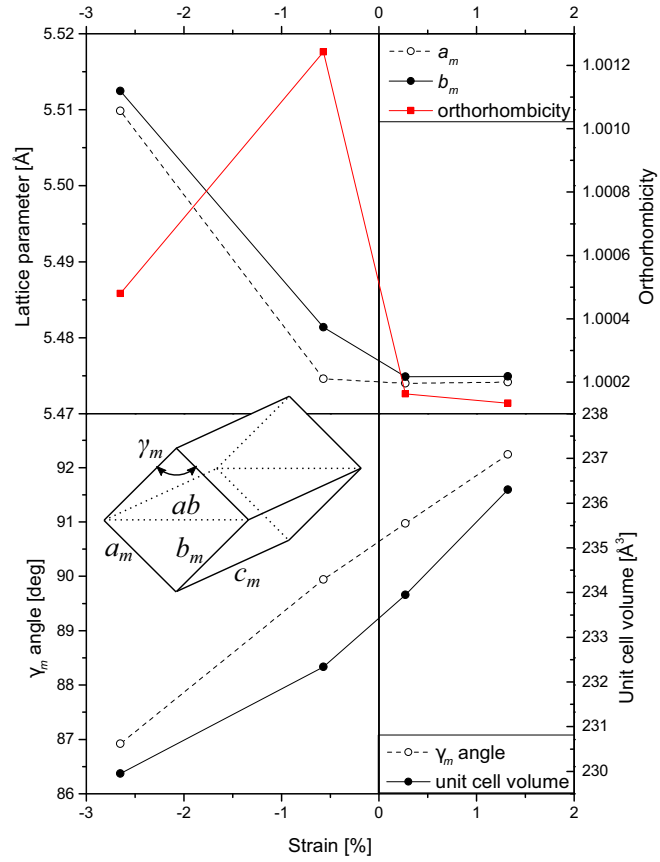

FIG. 1. Structural parameters of $La_{2/3}Sr_{1/3}MnO_3$ films as a function of in-plane strain along $[1\text{-}10]_m$ direction: a_m and b_m lattice parameters and orthorhombicity defined as b_m/a_m (top panel), γ_m angle and unit cell volume (bottom panel). Lines represent guides to the eye. The inset shows monoclinic unit cell, in which the lattice parameters are defined. The in-plane strain along $[1\text{-}10]_m$ direction was calculated from bulk value of LSMO ab distance $(ab)_{bulk} = 7.787$ Å [6] and measured ab values in Tab. I as $(ab - (ab)_{bulk})/(ab)_{bulk}$.

Having determined the crystallographic structure, we can characterize OOR in coherently strained LSMO films. The rotation patterns can be systematically described using the Glazer tilt notation system [40]. The OOR are expressed as a combination of three independent rotations around three pseudocubic axes: $[100]_{pc}$, $[010]_{pc}$, and $[001]_{pc}$. Relative magnitudes of the tilts are denoted by letters a, b, c and $+$ or $-$ superscripts denote either in-phase or out-of-phase rotations of two adjacent octahedra, 0 superscript means no rotation around the respective axis. Rhombohedral structure of bulk LSMO is described by tilt system #14 ($a^-a^-a^-$) [40], where rotations around all three axes are out of phase and they are all denoted by the same letter a, because they have the same relative magnitudes. As the epitaxial strain changes crystal structure of LSMO, it consequently changes the OOR pattern as well. It can be shown [6] that such distinction of structural properties of films grown under compressive and tensile strain, as described in the previous paragraph and shown in Fig. 1, leads to different OOR behavior. LSMO films under compressive strain can be described by tilt system #9 ($a^+a^-c^-$), while under tensile strain the OOR correspond to tilt system #18 ($a^+a^-c^0$). Both systems include in-phase

TABLE II. Parameters of the six electron transitions used to describe the optical response of $La_{2/3}Sr_{1/3}MnO_3$ films on four different substrates; A_n, E_n, and Γ_n for $n = 1, ..., 6$ stand for the amplitude, energy, and broadening of the oscillators, $\varepsilon_{1\infty}$ is the nondespersive term and E_g^* is energy of the pseudo bandgap determined from the third (Cody-Lorentz) oscillator.

Substrate	$\varepsilon_{1\infty}$	A_1	E_1 [eV]	Γ_1 [eV]	A_2	E_2 [eV]	Γ_2 [eV]	A_3	E_3 [eV]	Γ_3 [eV]	E_g^* [eV]	A_4	E_4 [eV]	Γ_4 [eV]	A_5	E_5 [eV]	Γ_5 [eV]	A_6	E_6 [eV]	Γ_6 [eV]
LAO	1.5	6.9	0.9	1.6	0.2	2.2	0.4	8.7	3.7	2.0	2.0	1.3	4.6	1.5	1.7	5.9	1.8	0.9	7.3	0.9
LSAT	1.4	14.1	0.6	1.4	0.2	2.2	0.4	5.2	3.8	1.8	1.7	1.8	4.4	1.6	0.6	5.3	1.0	2.0	6.7	1.2
STO	1.5	14.1	0.6	1.7	0.5	2.0	1.4	2.4	3.5	1.2	1.4	1.4	4.3	1.0	2.0	6.1	3.1	1.1	6.6	0.4
DSO	1.3	7.3	1.2	2.0	0.1	2.3	0.4	4.6	3.8	1.8	1.7	1.8	4.5	1.7	1.2	5.6	1.5	2.5	6.7	0.4

rotations around the *a* pseudocubic axis and out-of-phase rotations around the *b* pseudocubic axis. The difference is caused by the in-plane elongation under tensile strain. It results in suppression of rotations around the *c* pseudocubic axis, which are initially present in both bulk LSMO and films under compressive strain.

B. Optical characterization

Optical properties of the samples were characterized by means of spectroscopic ellipsometry. Measured spectra of ellipsometric angles were fitted to determine the diagonal elements ε_1 of permittivity tensor. They were parametrized as a sum of five damped Lorentz oscillators and one damped Cody-Lorentz oscillator, which served to determine energy of the pseudo bandgap E_g^*. Line shapes of the oscillators are described in detail in the Supplemental Material [18]. Amplitude A_n, energy E_n, and broadening Γ_n of each oscillator ($n = 1, \ldots, 6$) as well as the nondispersive term $\varepsilon_{1\infty}$ and pseudo bandgap energy E_g^* were adjusted by least-squares method. All the resulting parameters are displayed in Table II. Spectra of real and imaginary parts of the diagonal elements of permittivity tensor are shown in Fig. 2 for all samples.

The fits revealed six electronic transitions centered around approximately 0.8, 2.2, 3.7, 4.4, 5.6, and 6.8 eV. The main spectral features are the two transitions around 3.7 and 4.4 eV. They have already been reported in bulk LSMO [41] and polycrystalline films on silicon [42], as well as in single-crystalline thin films grown on STO [43] and LAO [44,45] substrates; however, they are most often described as one transition centered around 4 eV. This description is common in both optical [45] and magneto-optical [41,43] studies and the transition is assumed to be a charge transfer between O $2p$ and Mn $3d$ states. One magneto-optical study of LSMO on LAO [44] also supports the presence of two transitions at approximately 3.6 and 4.1 eV. Our theoretical approach using two transitions around the critical energy of 4 eV shows better agreement with experimental ellipsometric data. In spectra of samples deposited on STO and LAO, the two transitions can be clearly distinguished (see Supplemental Fig. S6 [18] for more details). This model is further supported by our magneto-optical investigation, which follows in the next section.

C. Magneto-optical characterization

MOKE spectroscopy was used to determine the off-diagonal elements of permittivity tensor ε_2 of the LSMO films. Room temperature spectra of Kerr rotation and Kerr ellipticity are displayed in Fig. 3. For clarity, spectra of the samples deposited on LAO and DSO are magnified by ten. The strong suppression of ferromagnetic ordering in these two films is caused by the large value of lattice mismatch and therefore large epitaxial strain. There are two mechanisms which are responsible for this behavior. First, the strain, both compressive and tensile, leads to distortion of the LSMO unit cell, which increasingly deviates from the bulk structure with optimized magnetic properties. Second, it has been shown that, at the LSMO/substrate interface, the DE interaction is suppressed as a result of preferential orbital ordering under

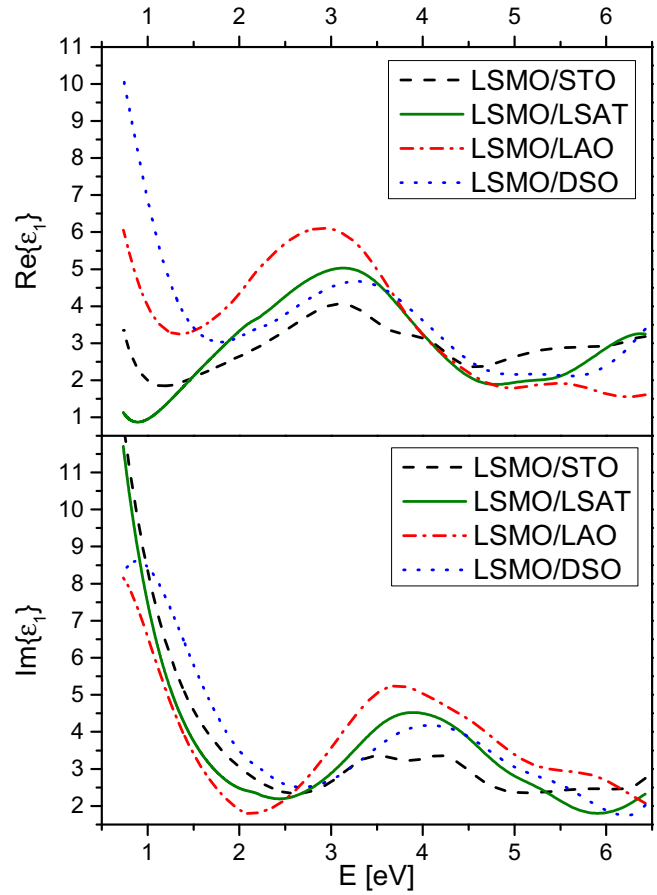

FIG. 2. Spectra of real and imaginary parts of the diagonal permittivity tensor elements of $La_{2/3}Sr_{1/3}MnO_3$ films on four different substrate materials, extracted from spectroscopic ellipsometry measurements.

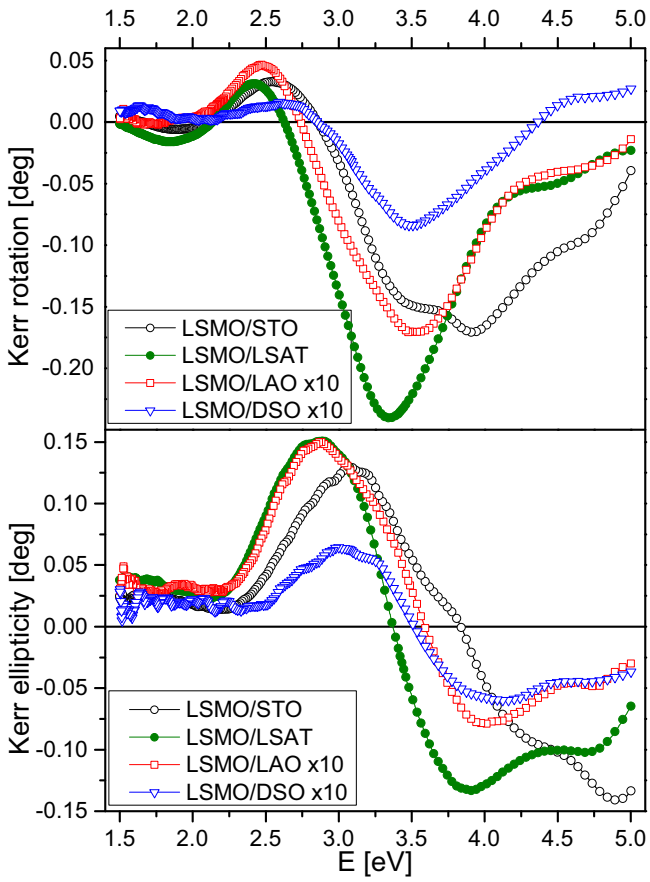

FIG. 3. Spectra of Kerr rotation and Kerr ellipticity of $La_{2/3}Sr_{1/3}MnO_3$ films on four different substrate materials. For clarity, spectra of samples deposited on LAO and DSO are magnified by ten.

epitaxial strain. This consequently leads to antiferromagnetic ordering near the interface, known as magnetically inert layer [46–48]. Combination of these effects further results in T_C decrease and lower magnetic moment of the films, as confirmed by both SQUID magnetometry and MOKE spectroscopy.

Electronic transitions, which form spectral dependence of the off-diagonal part of the permittivity tensor and hence are magneto-optically active, can be sorted into two types. Type-I transitions originate in spin-orbit splitting of the final states. The real part of such transition has a dissipative line shape; the imaginary part exhibits dispersive behavior. These transitions are called diamagnetic transitions for historical reasons [49]. On the other hand, type-II transitions arise from a difference in population of the spin-orbit split ground states. Their real part has a dispersive line shape while their imaginary part exhibits dissipative behavior. They are called paramagnetic transitions. Line shapes and parameters of the transitions are described in detail in the Supplemental Material [18].

The off-diagonal elements of permittivity tensor of our samples were calculated from MOKE spectra presented in Fig. 3 and from diagonal elements of permittivity tensor presented in Fig. 2 and Table II. The calculations were based on transfer matrix formalism [28]. Maximum amplitude $(\varepsilon_2^{'})_{\max}$ or $(\varepsilon_2^{''})_{\max}$, respectively, resonant frequency ω_0 and broadening Γ of employed oscillators were determined by least-squares method. The spectra were initially modeled as a sum of two electron transitions, whose presence has already been reported in LSMO thin films before. The most prominent spectral feature, which can be observed as a pronounced minimum around 3.6 eV in the Kerr rotation spectra in Fig. 3, has already been reported in bulk LSMO [41], polycrystalline films on silicon [42], as well as in single-crystalline thin films grown on STO [50,51] and LAO [44] substrates. It is related to charge transfer diamagnetic transition from O $2p$ states into Mn t_{2g} states in the minority spin channel. The second most prominent spectroscopic feature, visible as a maximum around 2.4 eV in the Kerr rotation spectra, is represented by crystal-field paramagnetic transition from Mn t_{2g} states into Mn e_g states in the majority spin channel. It has already been observed in LSMO grown on silicon [42], STO [50], and LAO [44] as well. These two transitions were sufficient to describe the off-diagonal elements of samples grown on STO and DSO substrates, i.e., grown under tensile strain. However, presence of a third electron transition was revealed around 4.3 eV in spectra of LSMO deposited on LAO and LSAT, i.e., under compressive strain.

It is difficult to identify presence of this transition in Kerr rotation spectra because the MOKE signal also contains optical response of the whole structure, including substrate. As amplitude of this transition is relatively small, its contribution to Kerr rotation spectra is not so evident. In case of the film grown on DSO, the Kerr rotation spectrum crosses the zero line at around 4.3 eV (see Fig. 3). In spectra of the films grown on LAO and LSAT, presence of the additional transition decreases spectral amplitude so the zero crossing at 4.3 eV is not visible. However, spectrum of the sample grown on STO markedly differs from the others due to above-mentioned complexity of MOKE signal. In this spectral region, a combination of high penetration depth of LSMO and the high reflectivity change of STO substrate results in strong optical contribution of the substrate to an overall MOKE signal. This effect has already been described by previous research [52]. To correctly interpret the MOKE spectra in terms of individual transitions, it is therefore necessary to perform a careful analysis of spectra of the off-diagonal permittivity tensor elements, which are directly related to the electronic structure. We present them in Fig. 4. Here the optical contribution of STO substrate is separated and the differences between compressively and tensilely strained films become clearer. The differences are commented in more detail in the Supplemental Material [18] (see Supplemental Figs. S7 and S8). Parameters of the transitions are given in Table III.

The exact origin of the third electronic transition around 4.3 eV has not been satisfactorily explained so far. The transition was observed by the group of Liu *et al.* [44] in LSMO films grown on (001) LAO substrates, i.e., under compressive strain, which is in agreement with our observations. According to Liu *et al.*, this transition occurs around 4.1 eV and it is assumed to be a charge-transfer diamagnetic transition from O $2p$ states into Mn t_{2g} states in the minority spin channel. This explanation seems unlikely given the temperature-dependent MOKE spectroscopy investigations performed by group of Rauer *et al.* [53]. They studied LSMO grown on (100) STO substrate, i.e., under tensile strain. They present

TABLE III. Parameters of the three electron transitions used to describe the magneto-optical response of $La_{2/3}Sr_{1/3}MnO_3$ films on four different substrates; $(\varepsilon_2^{'})_{max}$ or $(\varepsilon_2^{''})_{max}$, ω_0 and Γ stand for the maximum amplitude, resonant frequency, and broadening of the oscillators. The parameters were fitted from magneto-optical Kerr effect spectra presented in Fig. 3 with use of the diagonal permittivity tensor elements presented in Table II and Fig. 2.

Substrate	LAO	LSAT	STO	DSO
Transition 1		Crystal field transition Mn $t_{2g} \rightarrow e_g$		
$(\varepsilon_2^{''})_{max}$	0.010	0.472	0.069	0.001
ω_0 [eV]	2.45	2.50	2.38	2.49
Γ [eV]	0.43	0.66	0.38	0.42
Transition 2		Charge transfer transition O $2p \rightarrow$ Mn t_{2g}		
$(\varepsilon_2^{'})_{max}$	0.04	1.16	0.36	0.01
ω_0 [eV]	3.63	3.51	3.55	3.64
Γ [eV]	0.87	1.14	0.97	0.73
Transition 3		Crystal field transition Mn $t_{2g} \rightarrow e_g$		
$(\varepsilon_2^{''})_{max}$	−0.03	−0.69	No such	
ω_0 [eV]	4.26	4.25	transition under	
Γ [eV]	0.56	0.67	tensile strain	

off-diagonal elements of permittivity tensor in temperature range from 75 K to 330 K. The spectra measured at room temperature are in full agreement with our results, exhibiting two prominent spectral features around the same respective energies of 2.3 eV and 3.6 eV. With decreasing temperature, not only expected overall amplitude increment of the spectra is observed, but a clear signature of another spectral feature is revealed around energy of 4.3 eV. The shape and energy position of this transition is in agreement with the fits of our spectra measured on compressively strained LSMO, revealing this transition as paramagnetic. The temperature dependence of this transition further supports its classification as paramagnetic, in contradiction to the suggestion of Liu *et al.* We therefore assume that this paramagnetic transition originates in Mn t_{2g} levels in the majority spin channel. Occupation of these states can be influenced by both temperature or epitaxial strain, resulting in partial or full suppression of the observed electronic transition in MOKE spectra.

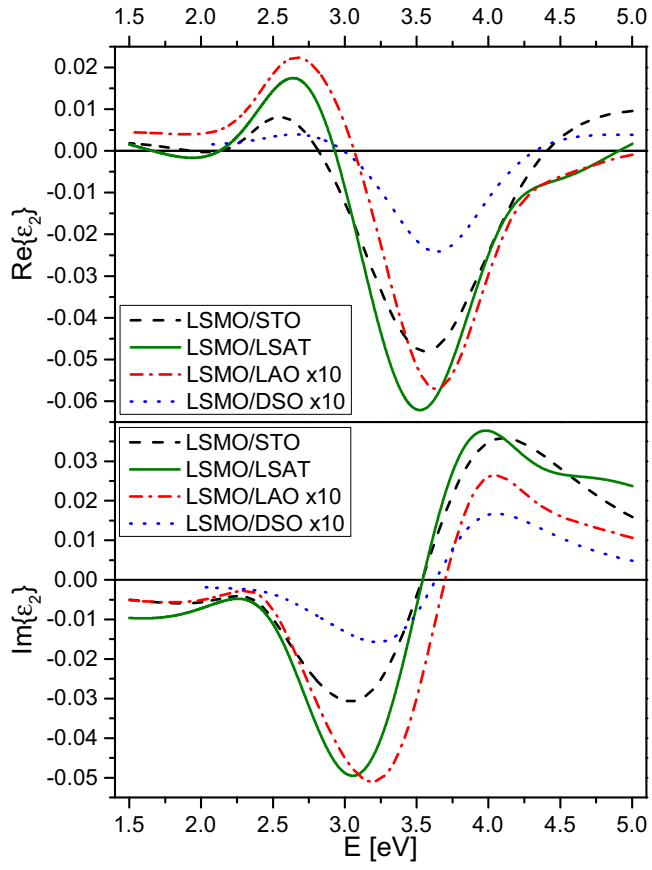

FIG. 4. Spectra of real and imaginary parts of the off-diagonal permittivity tensor elements of $La_{2/3}Sr_{1/3}MnO_3$ films on four different substrate materials, calculated from diagonal permittivity tensor elements and magneto-optical Kerr effect spectra. For clarity, the spectra of samples deposited on LAO and DSO are magnified by ten.

The work of Rauer *et al.* also allows us to make an important conclusion concerning OOR influence on resulting magneto-optical properties. We have shown that LSMO films exhibit different OOR behavior when grown under compressive and tensile strain. The presence of the third electronic transition in low-temperature spectra of films grown under tensile strain [53] therefore suggests that OOR is not the key parameter. The temperature change does not induce structural changes large enough to alter the tilt system. As the OOR remains the same with temperature while the third transition is induced, it indicates that OOR does not have a significant influence on magneto-optical properties of LSMO.

The proposed classification of the third electronic transition can be further supported in view of a study on LSMO electronic structure presented by Uba *et al.* [54]. Although their results about the exact electronic structure remained inconclusive in case of LSMO, they reported an optical interband Mn $t_{2g} \rightarrow e_g$ transition around 4.5 eV in the case of the LSMO parent compound $LaMnO_3$. Even though they did not find sufficient experimental evidence for this transition in their MOKE spectra measured on LSMO, they did find presence of the respective manganese orbitals at energies allowing this transition in DOS spectra of LSMO obtained by *ab initio* calculations. Other previously reported DOS calculations of

LSMO would support occurrence of this transition as well [23,24,44].

The last arguments in favor of the suggested electronic model consider magnitudes of the observed transitions and their optical activity. While the charge transfer diamagnetic O $2p \rightarrow$ Mn t_{2g} transition is the most prominent feature in observed MOKE spectra, both paramagnetic transitions have significantly smaller amplitudes, which supports their classification as Mn $d - d$ transitions. The fact that we observed the third transition (around 4.3 eV) in optical response of all LSMO samples, see Table II, Fig. 2, and Supplemental Fig. S6 [18], regardless of their strain state, indicates that magneto-optical activity of this transition is governed via occupation of the spin-orbit split Mn t_{2g} ground states. The occupation can be influenced by both temperature and epitaxial strain, leading either to enhancement or suppression of its magneto-optical activity. The first paramagnetic transition (around 2.4 eV) originating in the same ground state exhibits similar behavior, regarding both the temperature dependence [53] and the overall amplitude decrease under tensile strain (see Table III). Even though it is not fully suppressed under tensile strain, the amplitude is significantly diminished. The suppression is especially pronounced in the sample grown on DSO, i.e., under the largest tensile strain, which indicates strong sensitivity of the Mn t_{2g} levels on the epitaxial strain.

D. *Ab initio* calculations

To further investigate the influence of OOR and distortions on electronic structure of LSMO, we employed *ab initio* calculations. Bottom panel of Fig. 5 shows a comparison of total density of states (TDOS) calculated for bulk LSMO with rigid tilt system #23 ($a^0a^0a^0$) and bulk LSMO with tilt system ($a^-a^-c^-$). This theoretical tilt system only slightly deviates from the real rhombohedral tilt system #14 ($a^-a^-a^-$), concerning the tilt amplitude around $[001]_{pc}$ axis, due to simplified layered structure of LSMO used in the calculation. There are almost no visible changes in the TDOS spectral behavior except for the highest energy band located around 3 eV above Fermi level. This band is associated with La $4f$ states, which are not involved in observed magneto-optical transitions and, therefore, it will be omitted in further discussion. The negligible change of TDOS spectra suggests that magneto-optical transitions are not influenced by OOR. Several studies have pointed out that OOR engineering can be a successful way for tuning transport and magnetic properties of thin LSMO layers [9,11,13]. Liao *et al.* [12] even presented tuning of magnetic anisotropy by OOR and Kan *et al.* [10] achieved similar effect in thin films of $SrRuO_3$. Despite this clear evidence in favor of importance of OOR engineering, especially with respect to transport and magnetic properties of thin LSMO layers, on the other hand, our *ab initio* calculations imply that influence of OOR on TDOS spectra is negligible. This does not indicate an important role of OOR in influencing the magneto-optical properties, in agreement with previous observations following from the experimental results of Rauer *et al.* [53].

Based on the minor influence of OOR on TDOS spectra, the effect of strain was further studied in rigid oxygen octahedra system with no tilts. The top panel of Fig. 5 shows TDOS for bulk LSMO compared to two cases of LSMO strained in such a way that the pseudocubic c/a ratio corresponds to deposition on LAO and DSO substrates. The results are in agreement with previous findings of Ma *et al.* [23], i.e., there is no significant change of spectral shape; however, there is a visible shift of the spectrum to higher energies when going from compressive to tensile strain. Such shift itself would be insufficient to explain appearance of the third transition in MOKE spectra of compressively strained LSMO films. It is nonetheless well known that compressive or tensile strain leads via consequent octahedra distortions to different preferential orbital ordering in LSMO thin films [46,55–59]. Even though it is typically described as an interface effect explaining the DE suppression in LSMO layer near the substrate, it clearly demonstrates the sensitivity of Mn $3d$ levels to octahedra distortions. We therefore assume that the mechanism responsible for appearance of the third electronic transition in MOKE spectra of compressively strained LSMO is related to Mn $3d$ levels. As Mn t_{2g} levels in majority spin channel are the closest occupied states near the Fermi level, which are therefore most likely to be influenced by temperature,

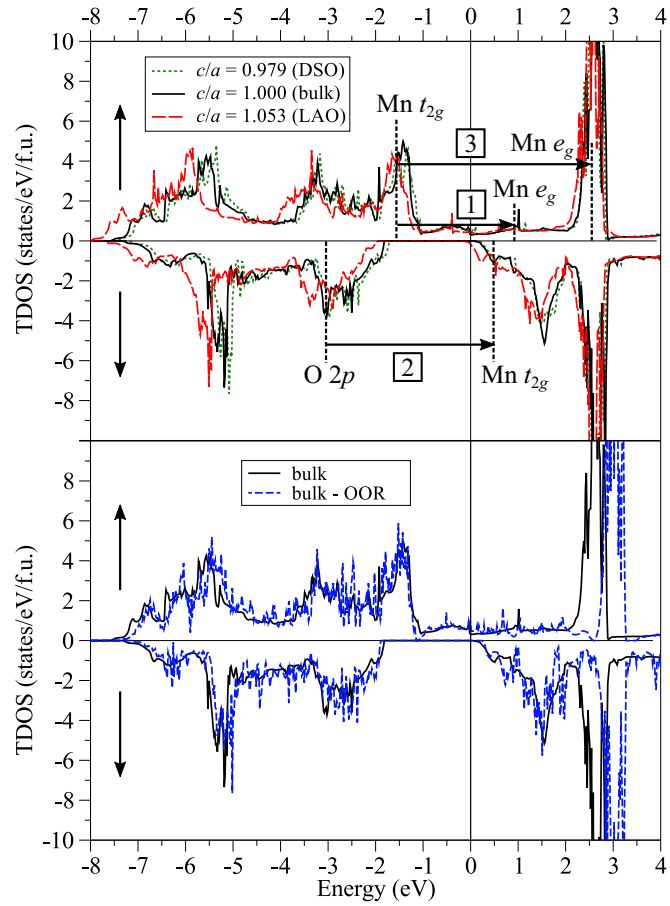

FIG. 5. Spectra of total density of states obtained by *ab initio* calculations. Top panel shows unstrained bulk LSMO and strained LSMO corresponding to growth on LAO and DSO substrates. Bottom panel shows bulk LSMO with no rotations of oxygen octahedra and bulk LSMO with quasireal tilt system ($a^-a^-c^-$).

we expect that the observed transition originates from these states.

Such findings are in agreement with arguments provided in the discussion in the previous section. The presented *ab initio* calculations therefore further support the suggested electronic model. They showed that the Mn t_{2g} level is most likely the ground state of the third electron transition. Moreover they confirm previous findings of other groups, which showed that location of Mn e_g bands is such that an interband Mn $t_{2g} \rightarrow e_g$ transition in the majority spin channel is possible around energy of 4.3 eV. We do not present here the element-resolved DOS; however, we indicate position of the Mn e_g band in the top panel of Fig. 5. The Mn e_g band partially overlaps with the La $4f$ band, but unlike the lanthanum band the manganese band is not affected by OOR. Therefore, we show that the observed paramagnetic transitions can unlikely be influenced by OOR engineering, but they can be suppressed or enhanced by changes in occupation of the Mn t_{2g} levels in the majority spin channel, which can be induced by temperature or strain-induced octahedra distortions.

The last argument that gives strong support for the suggested electronic model follows from direct comparison of experimental spectra of ε_2 presented in Fig. 4 with spectra of the off-diagonal elements of permittivity tensor obtained by *ab initio* calculations. The spectra were calculated from joint DOS and they are shown together with the experimental values in Fig. 6 for the cases of LAO and DSO substrates, which provide extreme values of the strain. A very good spectral agreement is clearly visible for both samples, demonstrating the validity of the approximations made in description of the LSMO unit cell in the *ab initio* calculations. All three discussed transitions can be recognized in the theoretical spectra at energies corresponding to their experimental values. The only larger difference can be seen at lower energies in spectra of LSMO on LAO. This is the region governed mainly by the first paramagnetic transition, which is therefore likely to be influenced by temperature. As the experimental spectra were obtained at room temperature while the *ab initio* calculations were performed at zero Kelvin, such disagreement could be expected. Region of the most prominent diamagnetic transition, which is not influenced by temperature, shows an excellent agreement with experimental spectra. It is easily seen on the main minimum in the real part and on the zero crossing near 3.6 eV in the imaginary part. High energies are governed by the third paramagnetic transition, which is again influenced by temperature. While in the experimental spectra the transition is visible only in LSMO/LAO (suppressed amplitude of imaginary part maximum, no zero crossing near 4.3 eV in the real part), in the theoretical spectra it is apparent for LSMO on both LAO and DSO. This clearly demonstrates that temperature is a key parameter for appearance of the third electronic transition. In agreement with experimental observations of Rauer *et al.* [53], our calculations show that the transition is visible at low temperatures even in MOKE spectra of tensilely strained LSMO films.

On the other hand, as OOR were left out in these calculations, our results in Fig. 6 demonstrate that the parameter of OOR is not necessary to be considered for description of magneto-optical response of LSMO, its influence is likely to be minor compared to the major role of octahedra distortions.

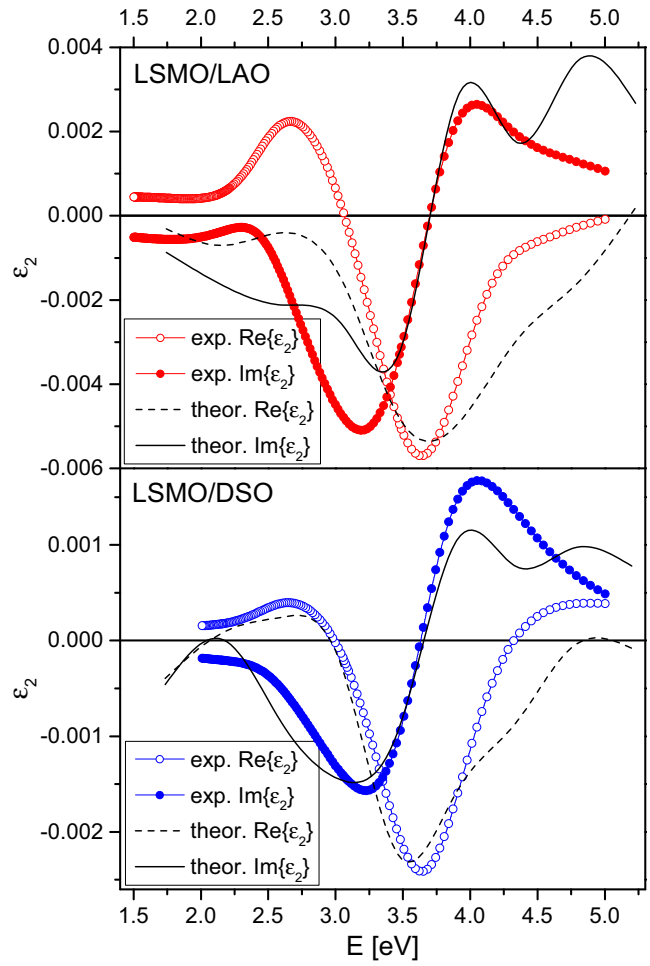

FIG. 6. Spectra of real and imaginary parts of the off-diagonal permittivity tensor elements of $La_{2/3}Sr_{1/3}MnO_3$ films deposited on LAO (top panel) and DSO (bottom panel) substrates. Spectra obtained experimentally by means of spectroscopic ellipsometry and magneto-optical spectroscopy are compared to spectra obtained theoretically by *ab initio* calculations. The theoretical spectra were multiplied by factors of 0.065 (LAO) and 0.020 (DSO) to compensate for the temperature-induced decrease of magnetization. The decrease is different for both samples, for which the factors also differ.

Such conclusion can be expected given the rotational symmetry of MnO_6 octahedron with respect to the manganese atoms. As can be seen from the TDOS spectra presented in Fig. 5, the energy positions of Mn levels in DOS spectra do not change under OOR. On the contrary, position of, for example, the La $4f$ states significantly changes as the OOR are not symmetrical with respect to the lanthanum atoms. As the observed magneto-optical transitions are governed by crystal field of the Mn atoms, which experience the rotational symmetry, it is then natural to expect no significant change of magneto-optical properties under OOR, leaving the octahedra distortions as a substantially more important parameter. The theoretical spectra of the off-diagonal elements of the permittivity tensor presented in Fig. 6 then fully justify this expectation, confirming the key role of temperature and oxygen octahedra distortions in controlling magneto-optical properties of LSMO.

IV. CONCLUSIONS

We performed a systematic study of the influence of epitaxial strain and OOR on the electronic structure of LSMO ultrathin films. SQUID magnetometry and MOKE spectroscopy confirmed deterioration of magnetic properties with increasing epitaxial strain, which can be explained by a combination of increasing unit cell distortion of the films and the magnetically inert layer. By combination of spectroscopic ellipsometry and MOKE spectroscopy, we determined the diagonal and off-diagonal elements of permittivity tensor. The spectra of the off-diagonal elements confirmed the presence of previously reported electronic transitions around 2.4 and 3.6 eV. A third electronic transition was observed around 4.3 eV only in spectra of films deposited under compressive strain. We proposed classification of this transition as a crystal-field paramagnetic transition from Mn t_{2g} to Mn e_g levels. Performed *ab initio* calculations further justified this classification and manifested a minor influence of OOR in comparison to the major role of octahedra distortions in determining magneto-optical properties of LSMO. We therefore demonstrated sensitivity of Mn $3d$ levels to oxygen octahedra distortions, leading to potential ways of tuning the magneto-optical properties of ultrathin LSMO films in future applications.

ACKNOWLEDGMENTS

This research was supported by Charles University, Project GA UK No. 68216. It was further supported by the Ministry of Education, Youth and Sports of Czech Republic by OP VVV Project MATFUN No. CZ.02.1.01/0.0/0.0/15_003/0000487 and by the Large Infrastructures for Research, Experimental Development and Innovations project IT4Innovations National Supercomputing Center_LM2015070. This work was also supported by a PHC Barrande grant of the French Ministry for Europe and Foreign Affairs, Project No. 34000QK. M.Z. and G.K. gratefully acknowledge the use of the SQUID magnetometer of the Physical Measurement Platform of Univ Paris-Sud, hosted by the Laboratoire de Physique des Solides (LPS, Orsay).

[1] R. von Helmolt, J. Wecker, B. Holzapfel, L. Schultz, and K. Samwer, Phys. Rev. Lett. **71**, 2331 (1993).
[2] G. H. Jonker and J. H. Van Santen, Physica **16**, 337 (1950).
[3] M. Bowen, M. Bibes, A. Barthélémy, J.-P. Contour, A. Anane, Y. Lemaître, and A. Fert, Appl. Phys. Lett. **82**, 233 (2003).
[4] C. Zener, Phys. Rev. **82**, 403 (1951).
[5] J. M. Rondinelli, S. J. May, and J. W. Freeland, MRS Bull. **37**, 261 (2012).
[6] A. Vailionis, H. Boschker, W. Siemons, E. P. Houwman, D. H. A. Blank, G. Rijnders, and G. Koster, Phys. Rev. B **83**, 064101 (2011).
[7] A. Vailionis, H. Boschker, Z. Liao, J. R. A. Smit, G. Rijnders, M. Huijben, and G. Koster, Appl. Phys. Lett. **105**, 131906 (2014).
[8] J. He, A. Borisevich, S. V. Kalinin, S. J. Pennycook, and S. T. Pantelides, Phys. Rev. Lett. **105**, 227203 (2010).
[9] Z. Li, D. Song, R. Yu, B. Ge, Z. Liao, Y. Li, S. Dong, and J. Zhu, ACS Appl. Mater. Interfaces **8**, 24192 (2016).
[10] D. Kan, R. Aso, R. Sato, M. Haruta, H. Kurata, and Y. Shimakawa, Nat. Mater. **15**, 432 (2016).
[11] X. Li, I. Lindfors-Vrejoiu, M. Ziese, A. Gloter, and P. A. van Aken, Sci. Rep. **7**, 40068 (2017).
[12] Z. Liao, M. Huijben, Z. Zhong, N. Gauquelin, S. Macke, R. J. Green, S. Van Aert, J. Verbeeck, G. Van Tendeloo, K. Held, G. A. Sawatzky, G. Koster, and G. Rijnders, Nat. Mater. **15**, 425 (2016).
[13] E. J. Moon, P. V. Balachandran, B. J. Kirby, D. J. Keavney, R. J. Sichel-Tissot, C. M. Schlepütz, E. Karapetrova, X. M. Cheng, J. M. Rondinelli, and S. J. May, Nano Lett. **14**, 2509 (2014).
[14] S. Thomas, B. Kuiper, J. Hu, J. Smit, Z. Liao, Z. Zhong, G. Rijnders, A. Vailionis, R. Wu, G. Koster, and J. Xia, Phys. Rev. Lett. **119**, 177203 (2017).
[15] N. M. Souza-Neto, A. Y. Ramos, H. C. N. Tolentino, E. Favre-Nicolin, and L. Ranno, Appl. Phys. Lett. **83**, 3587 (2003).
[16] N. M. Souza-Neto, A. Y. Ramos, H. C. N. Tolentino, E. Favre-Nicolin, and L. Ranno, Phys. Rev. B **70**, 174451 (2004).
[17] X. Ke, C. Adamo, D. G. Schlom, M. Bernhagen, R. Uecker, and P. Schiffer, Appl. Phys. Lett. **94**, 152503 (2009).
[18] See Supplemental Material at http://link.aps.org/supplemental/10.1103/PhysRevB.99.195138 for reciprocal space maps, SQUID magnetometry results, description of line shapes of electronic transitions, and description of LSMO unit cell in *ab initio* calculations. Supplemental Material includes Refs. [19–27].
[19] A.-M. Haghiri-Gosnet and J.-P. Renard, J. Phys. D **36**, R127 (2003).
[20] CompleteEASE Data Analysis Manual, version 4.63 (J. A. Woollam Co., Inc., 2011).
[21] A. S. Ferlauto, G. M. Ferreira, J. M. Pearce, C. R. Wronski, R. W. Collins, X. Deng, and G. Ganguly, J. Appl. Phys. **92**, 2424 (2002).
[22] F. J. Kahn, P. S. Pershan, and J. P. Remeika, Phys. Rev. **186**, 891 (1969).
[23] C. Ma, Z. Yang, and S. Picozzi, J. Phys.: Condens. Matter **18**, 7717 (2006).
[24] D. Petti, A. Stroppa, S. Picozzi, S. Brivio, M. Cantoni, and R. Bertacco, J. Magn. Magn. Mater. **324**, 2659 (2012).
[25] T. Bučko, J. Hafner, and J. G. Ángyán, J. Chem. Phys. **122**, 124508 (2005).
[26] O. H. Nielsen and R. M. Martin, Phys. Rev. Lett. **50**, 697 (1983).
[27] O. H. Nielsen and R. M. Martin, Phys. Rev. B **32**, 3780 (1985).
[28] P. Yeh, Surf. Sci. **96**, 41 (1980).
[29] G. Kresse and J. Furthmüller, Phys. Rev. B **54**, 11169 (1996).
[30] G. Kresse and J. Furthmüller, Comput. Mater. Sci. **6**, 15 (1996).
[31] P. E. Blöchl, Phys. Rev. B **50**, 17953 (1994).
[32] G. Kresse and D. Joubert, Phys. Rev. B **59**, 1758 (1999).
[33] J. P. Perdew, K. Burke, and M. Ernzerhof, Phys. Rev. Lett. **77**, 3865 (1996).
[34] J. P. Perdew, K. Burke, and M. Ernzerhof, Phys. Rev. Lett. **78**, 1396 (1997).
[35] S. L. Dudarev, G. A. Botton, S. Y. Savrasov, C. J. Humphreys, and A. P. Sutton, Phys. Rev. B **57**, 1505 (1998).

[36] P. E. Blöchl, O. Jepsen, and O. K. Andersen, Phys. Rev. B **49**, 16223 (1994).
[37] M. Gajdoš, K. Hummer, G. Kresse, J. Furthmüller, and F. Bechstedt, Phys. Rev. B **73**, 045112 (2006).
[38] M. C. Martin, G. Shirane, Y. Endoh, K. Hirota, Y. Moritomo, and Y. Tokura, Phys. Rev. B **53**, 14285 (1996).
[39] R. Tamazyan, S. van Smaalen, A. Arsenov, and Y. Mukovskii, Phys. Rev. B **66**, 224111 (2002).
[40] A. M. Glazer, Acta Cryst. B **28**, 3384 (1972).
[41] S. Yamaguchi, Y. Okimoto, K. Ishibashi, and Y. Tokura, Phys. Rev. B **58**, 6862 (1998).
[42] P. Thoma, M. Monecke, O.-M. Buja, D. Solonenko, R. Dudric, O.-T. Ciubotariu, M. Albrecht, I. G. Deac, R. Tetean, D. R. Zahn, and G. Salvan, Appl. Surf. Sci. **427**, 533 (2018).
[43] J. Mistrík, T. Yamaguchi, M. Veis, E. Lišková, Š. Višňovský, M. Koubaa, A.-M. Haghiri-Gosnet, P. Lecoeur, J.-P. Renard, W. Prellier, and B. Mercey, J. Appl. Phys. **99**, 08Q317 (2006).
[44] H. L. Liu, K. S. Lu, M. X. Kuo, L. Uba, S. Uba, L. M. Wang, and H.-T. Jeng, J. Appl. Phys. **99**, 043908 (2006).
[45] M. Quijada, J. Černe, J. R. Simpson, H. D. Drew, K. H. Ahn, A. J. Millis, R. Shreekala, R. Ramesh, M. Rajeswari, and T. Venkatesan, Phys. Rev. B **58**, 16093 (1998).
[46] A. Tebano, C. Aruta, S. Sanna, P. G. Medaglia, G. Balestrino, A. A. Sidorenko, R. De Renzi, G. Ghiringhelli, L. Braicovich, V. Bisogni, and N. B. Brookes, Phys. Rev. Lett. **100**, 137401 (2008).
[47] M.-B. Lepetit, B. Mercey, and C. Simon, Phys. Rev. Lett. **108**, 087202 (2012).
[48] M. Veis, M. Zahradnik, R. Antos, S. Visnovsky, P. Lecoeur, D. Esteve, S. Autier-Laurent, J.-P. Renard, and P. Beauvillain, Sci. Technol. Adv. Mater. **15**, 015001 (2014).
[49] C. J. Ballhausen, *Introduction to Ligand Field Theory* (McGraw-Hill Book Company, Inc., New York, 1962), p. 211.
[50] M. Veis, Optical interactions in thin films of selected magnetic oxides, Ph.D. thesis, Charles University, Prague, 2009, https://is.cuni.cz/webapps/zzp/detail/43481/35117740.
[51] M. Koubaa, A. M. Haghiri-Gosnet, J. P. Renard, M. Veis, V. Kolinsky, S. Visnovsky, Ph. Lecoeur, W. Prellier, and B. Mercey, J. Magn. Magn. Mater. **272**, 1812 (2004).
[52] M. Veis, Š. Višňovský, P. Lecoeur, A.-M. Haghiri-Gosnet, J.-P. Renard, P. Beauvillain, W. Prellier, B. Mercey, J. Mistrík, and T. Yamaguchi, J. Phys. D **42**, 195002 (2009).
[53] R. Rauer, G. Neuber, J. Kunze, J. Bäckström, M. Rübhausen, T. Walter, and K. Dörr, J. Magn. Magn. Mater. **290-291**, 948 (2005).
[54] L. Uba, S. Uba, L. P. Germash, L. V. Bekenov, and V. N. Antonov, Phys. Rev. B **85**, 125124 (2012).
[55] C. Aruta, G. Ghiringhelli, A. Tebano, N. G. Boggio, N. B. Brookes, P. G. Medaglia, and G. Balestrino, Phys. Rev. B **73**, 235121 (2006).
[56] C. Aruta, G. Balestrino, A. Tebano, G. Ghiringhelli, and N. B. Brookes, Europhys. Lett. **80**, 37003 (2007).
[57] A. Tebano, A. Orsini, P. G. Medaglia, D. Di Castro, G. Balestrino, B. Freelon, A. Bostwick, Y. J. Chang, G. Gaines, E. Rotenberg, and N. L. Saini, Phys. Rev. B **82**, 214407 (2010).
[58] D. Pesquera, G. Herranz, A. Barla, E. Pellegrin, F. Bondino, E. Magnano, F. Sánchez, and J. Fontcuberta, Nat. Commun. **3**, 1189 (2012).
[59] D. Pesquera, A. Barla, M. Wojcik, E. Jedryka, F. Bondino, E. Magnano, S. Nappini, D. Gutiérrez, G. Radaelli, G. Herranz, F. Sánchez, and J. Fontcuberta, Phys. Rev. Appl. **6**, 034004 (2016).